

Article



A comparison of damping-based methods to identify damage to carbon-fiber-reinforced polymers laminates subjected to low-velocity impact

Journal of Composite Materials 2024, Vol. 58(3) 401–417

© The Author(s) 2023
Article reuse guidelines: sagepub.com/journals-permissions
DOI: 10.1177/00219983231225451 journals.sagepub.com/home/jcm



Mohammad Rouhi Moghanlou, Ali Mahmoudi, MM Khonsari and G Li

Abstract

A method for detecting low-velocity impact damage in carbon fiber reinforced polymer (CFRP) is presented. It involves the use of the Impulse Excitation Technique (IET) and hysteresis loops to calculate the damping parameter of T700/NCT304-I carbon/epoxy samples subjected to various low-velocity impact energies. The value of the coefficient of restitution (COR) is determined for each impact, ranging between 0.62 for the lowest impact energy to 0.48 for the highest one. The results reveal that a three-step increase in the damping parameter exists in all cases as the impact energy on the specimen increases. An abrupt jump in the damping parameter value is observed for impact energies exceeding ~0.9 of the material's maximum capacity. Overall, at the highest impact energy equal to 3.65 J, the damping parameter increased by 43.3% compared to the pristine specimen. Additionally, two cases of cyclic tension-tension loading were applied to the specimens, with maximum stresses set at 150 MPa and 200 MPa. The measured values of plastic and elastic strain energy were used to determine the damping ratios. For both cases, the damping of the specimen subjected to the highest impact energy was ~1.2 times greater than that of an intact specimen, with an increase pattern similar to the findings of the IET method. Optical microscope images of the specimens are provided to illustrate various damage modes observed in the composite materials.

Keywords

Low-velocity impact, damping parameter, composites, fracture mechanics

Introduction

With the ever-growing demand for structures with high strength-to-weight ratios, fiber-reinforced polymers have become the material of choice for many design purposes. Carbon-fiber-reinforced polymers (CFRP) are, in particular, widely used in various industries, including aerospace, automotive, and sports equipment, because of their unique combination of desirable mechanical properties, such as high strength, lightweight, and durability. However, composite structures are susceptible to significant damage if exposed to external impact by foreign objects.

The damage caused by low-velocity impacts has been the subject of several articles on the mechanical properties of CFRP. Yang et al. developed FE models to predict the behavior of woven carbon/epoxy laminates during low-velocity impact and compression after impact (CAI), considering intra-laminar damage and inter-laminar delamination. Their models accurately predict load-displacement relations, failure modes, microscopic damage, and CAI

strength. Intra-laminar damage during impact was primarily initiated by tensile failure in the top ply. This study also found that residual compressive strength increased with decreasing impactor diameter, while CAI strength decreased by 34%–53% under impact energies. Another study investigated the growth of damage resulting from static indentation and low-velocity impact in cross-ply CFRP laminates. The researchers employed a drop-weight impact machine to examine the specimens experimentally and utilized two analytical models to assess the impact of

Department of Mechanical and Industrial Engineering, Louisiana State University, Baton Rouge, LA, United States

Corresponding author:

MM Khonsari, Department of Mechanical and Industrial Engineering, Louisiana State University, 3283 Patrick Taylor Hall, Baton Rouge, LA 70803, United States.

Email: khonsari@lsu.edu

Data Availability Statement included at the end of the article

transverse cracks on delamination propagation. The results revealed similar delamination propagation in both models, although there were variations in initial delamination stability and delamination shape. The ultimate delamination shape was notably affected by transverse cracks, leading to elongated delamination near the bottom layer. Damage to CFRP laminates from low-velocity impacts from the dropweight tower was examined in a separate investigation for low temperatures, down to -150°C . According to this study, cooling laminate prior to impact causes damage comparable to that caused by increasing impact energy, including deeper indentation, larger matrix cracking, and more severe fiber-matrix debonding and fracture.

In most metallic structures, damage manifests in a visible surface crack or local indentation. However, the complex state of internal damage often remains hidden in composites, so an abrupt failure is not uncommon. 10-14 Ultrasonic testing is one of the most common NDT techniques for identifying damage in CFRP components. Shen et al. studied several ultrasonic testing methods to identify impact damage in CFRP laminates. Common strategies like pulseecho and through-transmission are covered, along with more sophisticated ones like polar scattering, methods that are thickness-independent, air-coupled testing, and ultrasonic Rayleigh and Lamb Waves. Their research demonstrates that a non-destructive ultrasonic method can detect inner matrix cracks and delamination effectively. The pulseecho mode works effectively for thinner samples, but thickness segmentation is required for multi-layered specimens. Two distinct ultrasonic testing techniques for characterizing CFRP structures were covered in an article by Helfen et al. 15 Their results showed that the sampling phased array (SPA) method can be used to improve spatial resolution in real-time imaging as well as to detect and size a variety of component defects. In the cases where early damage detection is favorable, which could take the form of microcracks, non-linear ultrasonic transmission method was recommended. Additionally, technologies such X-radiography, digital image correlation, and infrared thermography are examples of other methods used to detect various flaws, including matrix cracking, delamination, fiber/matrix interfacial debonding, fiber fracture, or fiber waviness. 16-18

A powerful, non-destructive method for examining damage is to evaluate the damping parameter. ^{19,20} The damping parameter, also known as the damping ratio, is a measure of the amount of energy dissipation in a material due to external forces. The damping ratio affects the rate of decay of vibrations and thus influences the stability, durability, and performance of composite structures. ^{21–23} A review paper by Treviso et al. summarizes the available literature on damping in composite materials. The review emphasizes the importance of choosing the correct damping model based on the problem configuration and availability

of input parameters.²¹ The authors suggest that experimental characterization of composites' dynamic properties is still far from being standardized an' that further research is needed to improve our understanding of the energy dissipation mechanisms in composite materials.²¹

Experimental studies on the damping behavior of composites have been conducted using various techniques. such as dynamic mechanical analysis, modal analysis, and impact testing. These studies have shown that the damping factor of composite structures can vary depending on the frequency of vibration, temperature, and moisture content. 24,25 Additionally, it has been reported that the damping of composites may increase or decrease with increasing frequency, depending on the thickness of the specimen.²⁶ The vibration damping characteristics of CFRP hybrid composites and nanocomposites containing multiwall carbon nanotubes (CNTs) were investigated by Khan et al. ²⁷ They showed that the damping ratio rose as the CNT content increased, supporting the idea that there are boundary and interfacial sliding at the CNT-matrix. Compared to neat epoxy, CFRP composites displayed a higher rate of increase despite having a lower damping ratio.

A method for spotting cracks in composite structures is the damping parameter. Kyriazoglou et al.²⁸ examined the differences between CFRP and GFRP damping behaviors. Their study shows that fatigue causes damage to CFRP laminates' outer plies, whereas GFRP woven laminates sustain minimal damage in their outer plies prior to failure. The results revealed that it is important to track the damping capacity to spot any damages before severe damage mechanisms occur, as cracks can alter the damping properties of the material. A similar technique has been employed by Yam et al. to detect delamination in composite structures.²⁹

Kiral et al. investigated the response of composite beams under single-impact loading, explicitly focusing on the natural frequency and damping ratio variations. 30 They used an impact test to create failures of different sizes on the beam and recorded free vibration responses using a non-contact vibration measurement system. The damping ratio was calculated using the exponent of the free vibration envelope and the logarithmic decrement. They noted that the variation in the natural frequency value is not steady or measurable for the considered failure cases and is affected by the severity and location of the damage. It was observed in another study that damage in a cantilever beam causes a reduction in its natural frequencies, which disappears as the failure moves away from the clamped edge.³¹ Berthelot evaluated damping in rectangular laminated plates using the Ritz method. The method involves expressing the transverse displacement of the plates as a double series of the in-plane coordinates to evaluate the strain energies stored in each layer of the laminates.³² The damping characteristics of the laminates were evaluated experimentally using cantilever beam specimens, and the results showed a significant increase

in material damping with frequency. The damping evaluation based on the Ritz method was applied to different beam and plate configurations, and it was observed that the fiber orientation and ply stacking sequences influenced the damping properties. The beam and plate damping were also found to be dependent on the vibration modes and mode shapes.³² An increase in the damping parameter by the damage in the material has already been experimentally and numerically shown, but the extendibility of this non-destructive testing model in low-velocity impact cases is still unclear.^{33,34}

In this study, T700/NCT304 CFRP specimens were subjected to low-velocity impact tests at different energy levels. The maximum allowable energy for the specimen, also known as impact resistance, was determined by conducting impact tests at different energies. The aim here is to represent the damage from low-velocity impacts by means of the damping properties and establish a correlation between the input impact energy and the damping coefficient. For this purpose, the Impulse Excitation Technique (IET) was implemented using the Resonant Frequency Damping Analyzer (RFDA) device, which measures the resonant frequencies along with the damping coefficient of a specimen using the vibration of the material under a mechanical impulse trigger.

Theoretical background

This section presents the theory behind the damping parameter calculation using the IET method. Similar to

properties like density or thermal conductivity, damping is a material parameter that must be determined experimentally. This parameter is not a function of the geometry of the material, but depends on the external variables (including temperature) and varies as damage is propagated inside the structure of the material. 35,36 Different definitions and procedures exist for damping calculation in a material subjected to external vibration. However, internal damping, Q^{-1} , is the measurement method in IET method. The basis for the internal damping in a material is the energy dissipation through mechanical processes in response to external forces that may include vibration, fatigue, or impact loads. 37,38 This method calculates the damping parameter using the so-called loss-factor (η) parameter. Obtained via the logarithmic decrement method, damping is measured by dividing the total energy dissipation by the maximum elastic energy of the material.³⁹ Figure 1 illustrates the response of a damped and an undamped system. A_i values in this curve represent the peaks of vibration response through time, and their ratio enables one to identify the intensity of damping in the structure.

The specimen is externally excited to apply the IET method, and a vibrational response is collected for analysis. The response is represented by a signal-time curve that exhibits diverse shapes depending on the material's properties. A method to calculate the damping is by solving the general equation of motion for a single degree of freedom damped system:

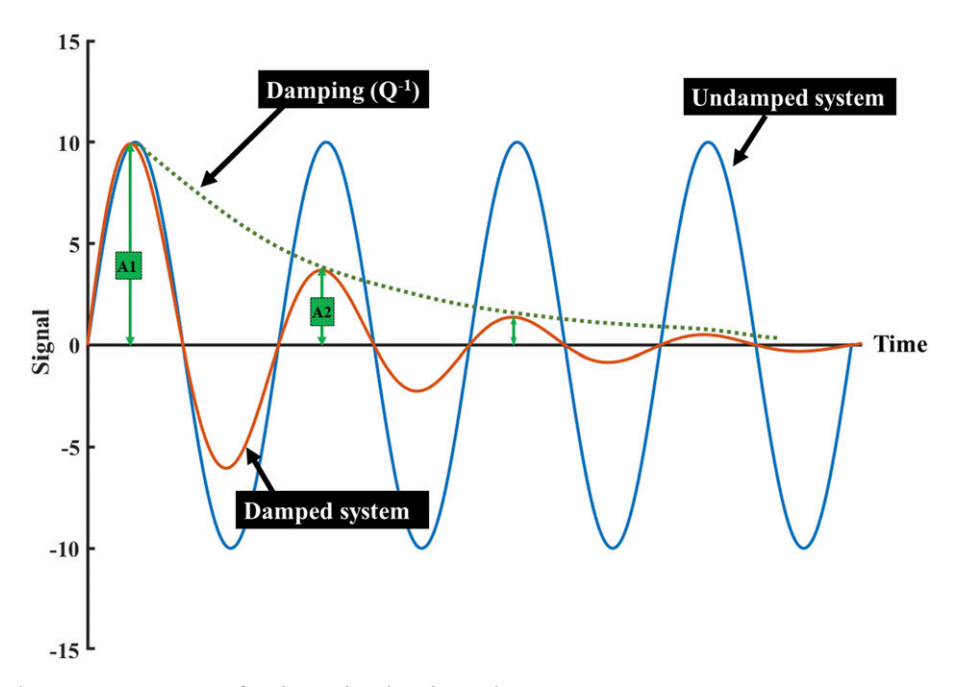


Figure 1. A signal-time response curve for damped and undamped systems.

$$m\frac{d^2y}{dt^2} + c\frac{dy}{dt} + ky = 0 \tag{1}$$

where m is the mass of the system, c is the viscous damping constant, and k is the spring constant. A well-known approach to solving this equation is by defining two variables λ and ω_n dependent on m, c, and k.

$$\frac{d^2y}{dt^2} + 2\lambda\omega_n \frac{dy}{dt} + \omega_n^2 y = 0$$
 (2)

where λ and ω_n are defined as follows:

$$\begin{cases} \lambda = \frac{c}{2\sqrt{km}} \\ \omega_n = \sqrt{\frac{k}{m}} \end{cases}$$
 (3)

The solution for the equation above is:

$$v(t)Ae^{-\lambda t}\sin\left(wt+\varphi\right)\tag{4}$$

where A represents the amplitudes of the input signal throughout the oscillatory response, φ is the phase angle and

$$w = \omega_n \sqrt{1 - \lambda^2} \tag{5}$$

The logarithmic decrement, δ , is defined as the logarithmic ratio of any two consecutive signal peaks, A_i , as given below:

$$\delta = \frac{1}{n} \ln \left(\frac{A(t)}{A(t+nT)} \right) = \ln \left(\frac{A_i}{A_{i+1}} \right) \tag{6}$$

where T is the time period and A_i is the ith peak of the input signal, as shown in Figure 1. The damping ratio, ζ , is defined in terms of δ as shown below:

$$\delta = \frac{2\pi\zeta}{\sqrt{1-\zeta^2}} \to \zeta = \frac{\delta}{\sqrt{4\pi^2 + \delta^2}} \tag{7}$$

When the damping ratio is small, typically $\zeta < 0.2$, ³⁶ by integrating equations (6) and (7), following formulas are obtained:

$$\sqrt{1-\zeta^2} \sim 1 \to \delta = 2\pi\zeta \tag{8}$$

$$\zeta = \frac{\delta}{2\pi} = \frac{\ln\left(\frac{A_i}{A_{i+1}}\right)}{2\pi} \tag{9}$$

Using the above equation, the damping ratio can be calculated for a given vibration response (as illustrated in Figure 1). Because the damping ratio is determined by fitting

the entire signal envelope, inaccurate peak signal values make precise vibration response collection essential to this method.

Additionally, the Q factor, i.e., the ratio of stored energy in the system to the dissipated energy, is also determined based on the damping ratio according to the following formula:

$$Q = \frac{1}{2\zeta} \tag{10}$$

This equation can be converted to define the internal friction, Q^{-1} , as below:

$$Q^{-1} = 2\zeta = \frac{\delta}{\pi} = \frac{\Delta E_{Total}}{2\pi E_s} \tag{11}$$

where ΔE_{Total} represents the total dissipated energy and E_s is the stored energy in the material. Given the signal-time curve of a sample freely vibrating in the IET method, the values for damping can be calculated using equation (9) provided that ζ remain below 0.2.

Material and experimental setup

In this section, first, the geometry and mechanical properties of the specimen are introduced. Then the procedures for performing low-velocity impact tests and calculating damping coefficients are described. Also described is the process of obtaining hysteresis loops using low-stress, fully reversed fatigue tests.

Material and specimen preparation

Specimens are prepared from CFRP sheets (DragonPlate, ALLRed & Associates Inc.) consisting of six unidirectional T700 carbon fiber laminas and NCT 304-1 resin. All six layers have the same 0° orientation along the longitudinal axis and each layer has a thickness of 0.28 mm with a total thickness of 1.70 mm in each sheet. The fiber's orientation allows for the specimen's maximum tensile and bending stiffness. Figure 2 illustrates the specimen's geometry and the orientation of laminas inside it. It should be noted that during the production of the laminates, a woven outer layer has been added to the surface of the composite sheets to increase their integrity and adhesiveness. The specimens are tabbed at both ends with the same composite material and dimensions of 8.5 × 25 mm to alleviate the stress concentration at the gripping section. T700 fibers have a tensile strength of 4825 MPa. With the unidirectional orientation of fibers in this specimen, UTS in the 0° direction is 2400 MPa, while in the 90° orientation it is 94 MPa based on manufactorer's datasheet. The mechanical properties of the CFRP

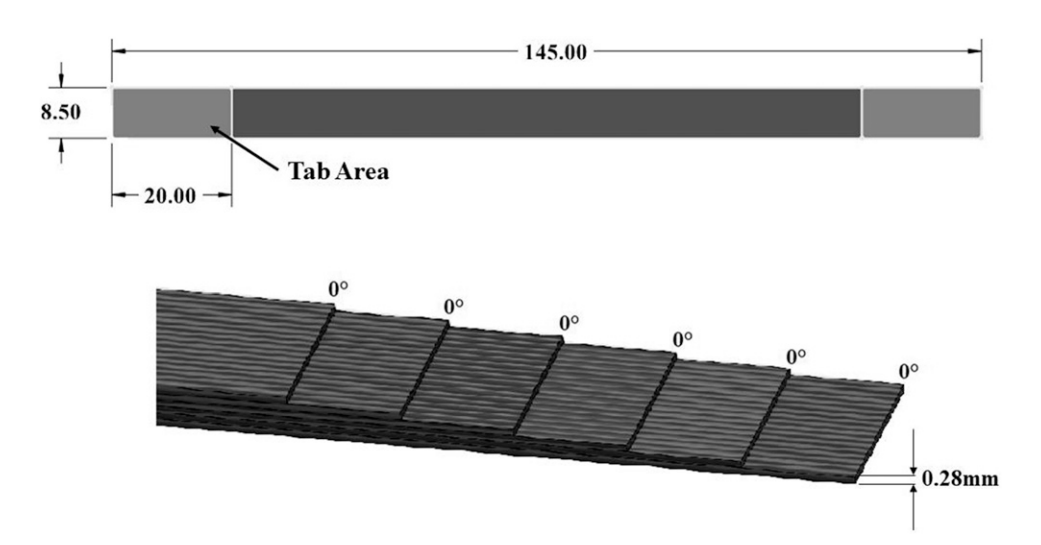


Figure 2. Geometry and lamina orientation of T700/NCT304-I CFRP specimens (dimensions in mm).

Table I. Material parameters of T700/NCT304-I carbon/epoxy samples.

Parameters	T700/NCT304-		
E _{m11} ^a	124.51 GPa		
E _{m22} ^a	8.3 GPa		
$v_{12} \& v_{13}^{b}$	0.29		
UTS 0°b	2400 MPa		
UTS 90°b	94 MPa		
Ply thickness ^a	0.28 mm		
$ ho^{b}$	1550 kg/m ³		
Fiber volume fraction ^b	55%		

^aExpermentally evaluated.

samples used in this work are provided in Table 1. It should be noted that values of E_{m11} and E_{m22} are experimentally obtained by simple tensile testing in the elastic zone.

Impact test

In this section, the process of performing low-velocity impact tests is described. An impact with a maximum velocity of 10 m/s is considered a low-velocity impact. However, a low-velocity impact is not necessarily classified as low-energy since the impact energy is proportional to the mass of the dropped object and if the mass is substantial, the produced impact energy would be considerable. A schematic of the low-velocity impact device used in this research

is shown in Figure 3. As seen in this figure, guiding columns with a height of 2 m, made of an aluminum alloy, are holding the dropping frame, which is a plane with an electrical magnet. The magnet is a 12V DC solenoid that can hold up to 100 N loads. The impactor ball is placed below the specified location in the plane and falls as the magnet power is turned off. There is a 16×8 cm fixture at the bottom of the device to hold the specimen, as can be seen in the figure.

Assuming that there is no energy dissipation due to friction, the impact energy of a free-falling ball can be estimated from the kinetic energy equation $E = 0.5m(v_1^2 - v_0^2)$, where v_1 and v_0 are the initial and final velocities of the impacting ball. In the current work, as the height of the impactor is a variable parameter in the experiments, the potential energy equation is used to calculate the input energy of the system. The equation for the input impact energy is as follows:

$$E = mgh (12)$$

where m is the mass of the impactor ball and h is the height of the drop weight frame. The drop-weight impactor ball is spherical and made of AISI 52100 Chrome steel. The diameter of the ball is 38 mm, and its weight is 226 g. Given the mass of the steel ball and the limit in the height of the impact device at 2 m, using the law of conservation of energy, the maximum velocity of the ball is 6.2 m/s, which falls into the category of low-velocity impacts. Accordingly, the highest impact energy achievable with this configuration is 4.4 J, which is

^bProvided my manufacturer.

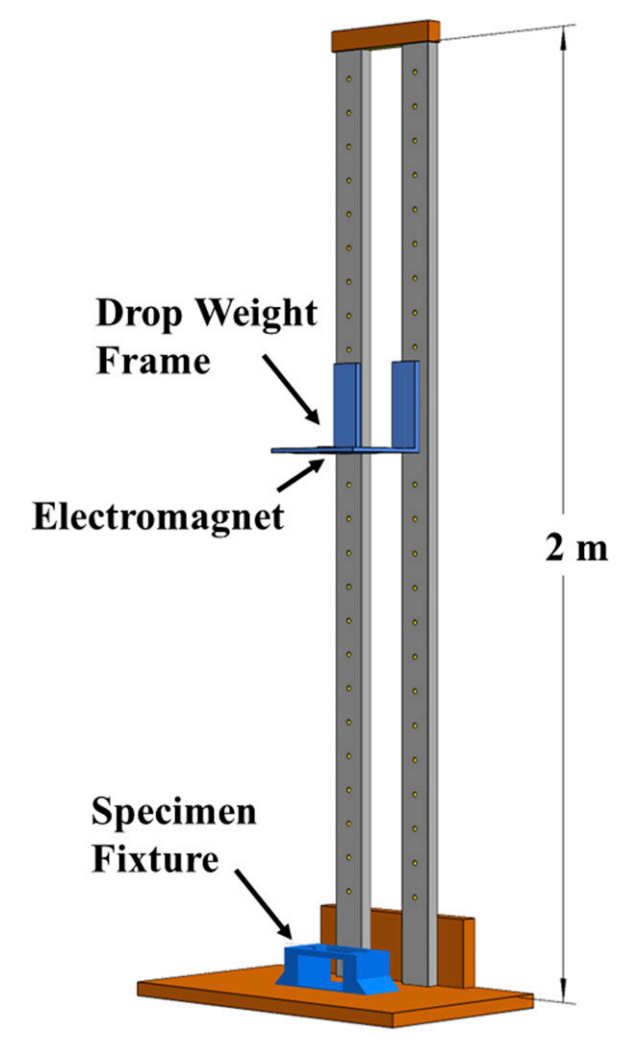


Figure 3. Drop-weight low-velocity impact device.

adequate for fracturing the specimens (see Low-velocity impact section).

It should be noted that there is no lower limit for the impact energy on the material since the height and weight of the dropping ball can be lowered to the desired amounts if needed. Figure 4 illustrates the damage mechanisms in CFRP specimens under low-velocity impact incidents. While fiber breakage in outer layers indicates total failure in the material, delamination and matrix cracks through inner layers may remain unnoticed while reducing the structural strength of the material.⁴⁴

Damping and fatigue tests

The RFDA device (IMCE, Belgium) used for measuring damping is a non-destructive material characterization device. It implements the IET method to obtain the acoustic information from the samples, and its software computes the resonant frequencies of the material in the range of 10 Hz to 16 kHz with the respective damping coefficients. This method relies on the dependence of resonant frequencies of an impulse-excited material on the geometry and stiffness properties. Figure 5 shows the schematic of the RFDA device used in this research along with a typical signal response of the experiment used to calculate the damping. Two metal strings hold the sample while allowing it to have the free-free vibration modes when manually triggered using a hammer with an elastic handle and a metallic spherical impactor provided with the RFDA device. Specimens are placed above the strings, and by manually tapping them using the hammer, the vibrational response of the material is collected by the microphone and sent to the

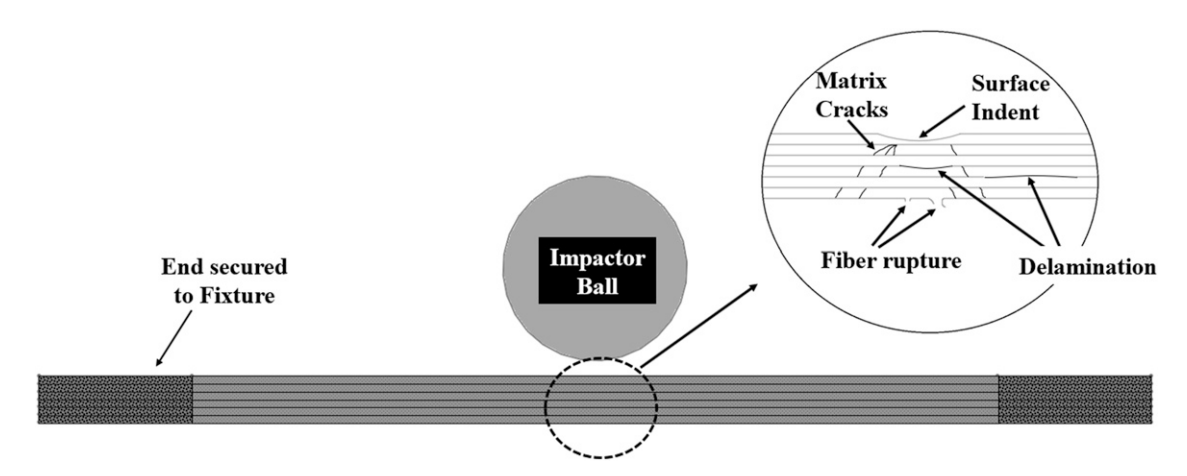


Figure 4. Different damage mechanisms in a sample subjected to low-velocity impact: delamination, fiber breakage, matrix cracking and surface indentation.

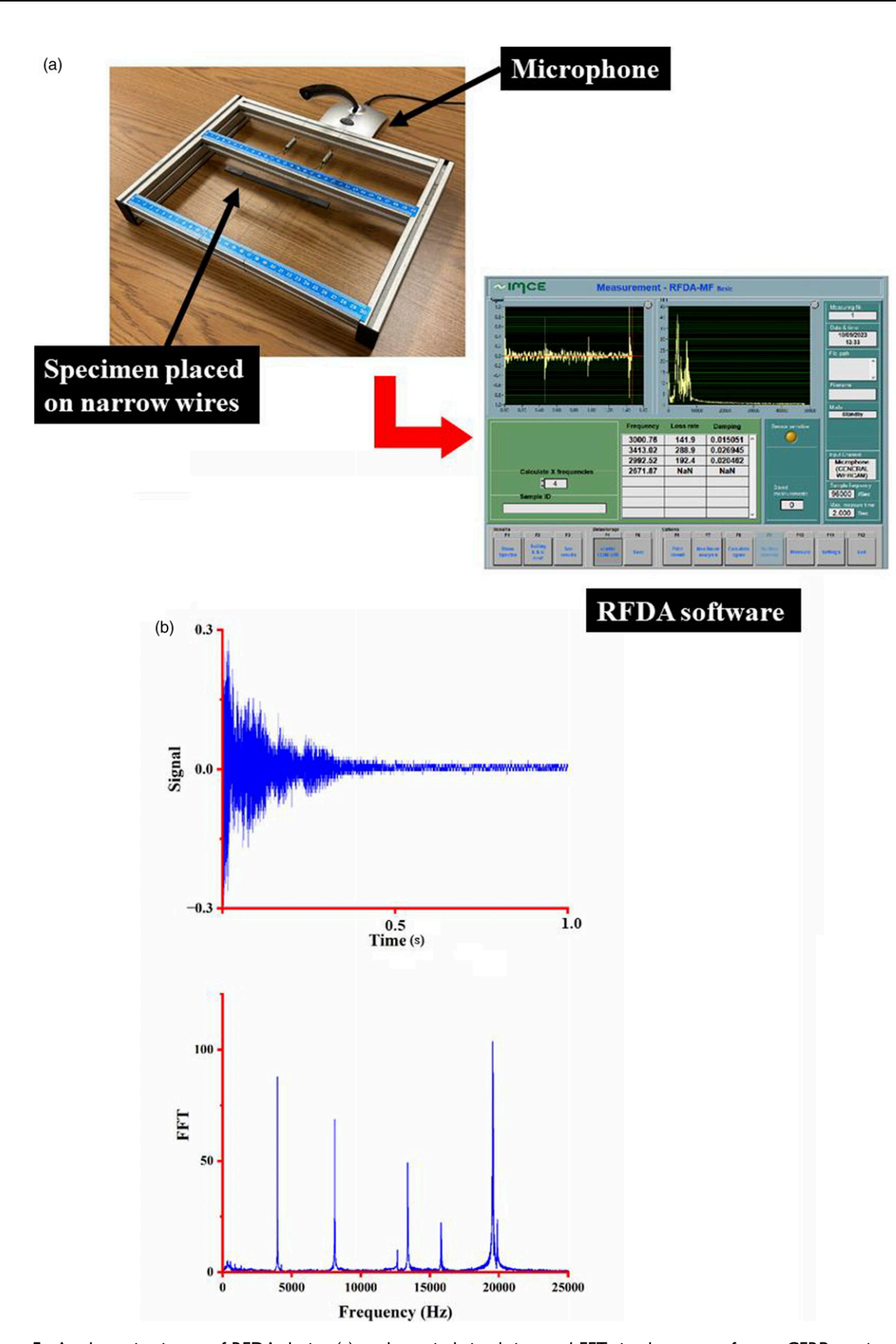


Figure 5. A schematic picture of RFDA device (a), and a typical signal-time and FFT-signal response from a CFRP specimen (b).

RFDA software, where the resonant frequencies and respective damping parameters, along with Young's modulus and Poisson's ratio of the sample are calculated using the ASTM E1876-15 standard. Figure 5(b) presents a typical signal-time response of the specimen's mechanical vibration. This graph's signal decay rate versus time represents the damping parameter. In addition, the material's natural (resonant) frequency was determined using the Fast Fourier Transform (FFT) of the input signal. To perform damping experiments, an appropriate environment is needed to ensure that the external sources of vibration and undesired noises do not interfere with the signal received by the device. As stated in Section 2, precision in data collection using this method ensures that the damping calculations are done correctly. In the RFDA device, the sample collection frequency rate is 96000 times per second, ensuring that all signal-time graph peaks are gathered.

Cyclic stress-strain response of specimens (Hysteresis loops) was obtained using a tension-compression fatigue device (TESTRESOURCES, USA) and axial extensometer for collecting the generated strains under each load.

Results and discussion

Low-velocity impact

Each specimen was initially subjected to low-velocity impact with different drop heights. Table 2 illustrates the impactor height and the velocity and input energy of the impact on the specimen. Since the impactor mass is equal to 226 g, the impact energy directly correlates with the dropping height. Seven (7) different impact energies are tested in this work. One specimen, No. 1, was left intact and used as a reference in the following sections to compare the

damping responses. As can be seen in Table 2, it was found that the maximum impact energy at fracture for this material equals $E_{\rm max}=3.65~\rm J$. The lowest impact energy, related to the drop height of 88 cm, is equal to 53.1% of the maximum impact energy of the specimen. There were no additional experiments below this energy level, as it has been shown that the damage in composite materials generally has a nonlinear behavior. This means that most damage occurs when the energy is near its limits, and a relatively large portion of impact energies do not damage the material structure. 45

As expected during the experiments, the ball tends to bounce back after hitting the specimen due to the elastic response of the material that does not completely keep all the input energy of the impact. The coefficient of restitution (COR) is a parameter that defines the intensity of this response. If the specimen were to absorb all the impact energy, then COR would be zero, i.e., perfectly plastic impact. The equation for calculating the coefficient of restitution, *e*, is:

$$e = \frac{|V_{1f} - V_{2f}|}{|V_{1i} - V_{2i}|} \tag{13}$$

where $V_{1\rm f}$ and $V_{2\rm f}$ are the final velocities of two objects after the impact and $V_{1\rm i}$ and $V_{2\rm i}$ are the initial velocities of objects before the impact happens. The impact may cause transient vibrations in the first few milliseconds, but their effect is mitigated by the specimen's small displacement, which diminishes with distance from the midpoint. As the second object is stationary, only the before and after velocities of the impactor ball are considered. So, the equation can be written as the ratio between the final and initial velocities of the ball. Based on the energy conservation law,

Table 2.	Low-velocity	impact	properties	of	specimens.

Specimen no.	Height (m)	Impact velocity (m/s)	Energy (J)	Max. Energy fraction (%)	
I	0	0	0	0	
2	0.88	4.15	1.94	53.1	
3	1.05	4.53	2.32	63.5	
4	1.20	4.85	2.65	72.6	
5	1.35	5.14	2.98	81.6	
6	1.55	5.51	3.43	93.9	
7	1.60	5.60	3.54	96.8	
8 (failed)	1.65	5.68	3.65	100	

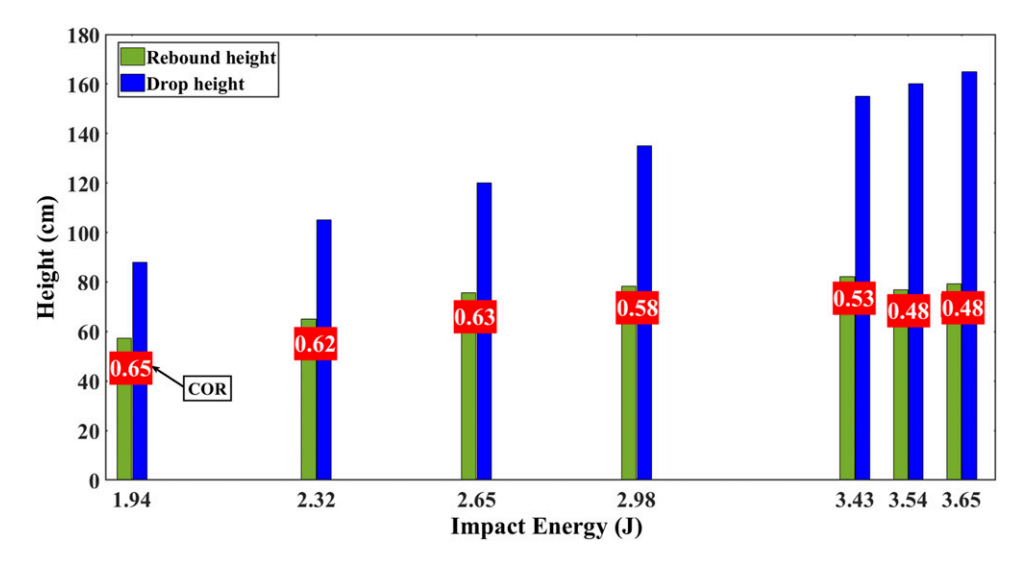


Figure 6. Drop and rebound heights as well as COR for low-velocity impacts.

 $\frac{1}{2}mv^2 = mgh$, the ratio between the velocities before and after impact is correlated with the root of the ratio between heights. As a result, COR can be calculated from the root of the ratio between the height of bounce back and the initial height:

$$e = \frac{|V_{1f}|}{|V_{1i}|} = \sqrt{\frac{h_f}{h_i}}$$
 (14)

where h_f and h_i are the bounce-back and initial heights, respectively. Using a high frame rate camera, the bounce-back height was collected during the experiments and is reported in Figure 6, along with the COR for all the low-velocity impact cases. As can be observed, the value of this coefficient decreases as impact energy approaches the final value, suggesting that a higher percentage of the input energy is being converted into internal energy absorbed by the specimen and results in the generation of damaging and (slightly) localized heat on the impact zone.

Figure 7 shows the magnified images of the surface and side views of specimen No. 1 (pristine specimen). As mentioned earlier, the woven surface layer of the specimen can be seen in Figure 7(a). Inner fibers of carbon are shown in Figure 7(b). As mentioned in the material properties, are all in 0° direction. Each layer in Figure 7(c) is measured to be in the range of ~290–315 µm as indicated by the manufacturer, including the

thin layer of resin between the laminas. The impact region on the surface and the side and opposite surfaces of specimen No. 8, which failed during the low-velocity impact with an energy of E = 3.65 J, are all shown in Figure 8. Figure 8(a) depicts the surface indentation damage, Figure 8(b) shows the transverse cracks and fiber layer delamination within the specimen, and Figure 8(c) shows the rupture of the fibers.

Damping calculation

As explained in Section 3, all the specimens, including the pristine specimen (no impact), were examined using the RFDA device by manually exciting the specimen and gathering the information using a microphone. For each specimen, the damping calculation was repeated 15 times, and the mean value, along with the standard deviation (SD) of the damping coefficient, is presented in Table 3. Additionally, Natural frequencies were calculated using RFDA software. It was observed that those frequencies generally remain consistent throughout multiple tests in a given impact energy and slightly increase as the impact energy increases. For sample No. 1, the first natural frequency was equal to 502.82 Hz. For the specimen subjected to an impact energy of E = 3.54 J, the measured frequency was 513.63 Hz, indicating a 2.1% increase. However, the variations of frequency were not significant enough to be considered a reliable indicator of damage

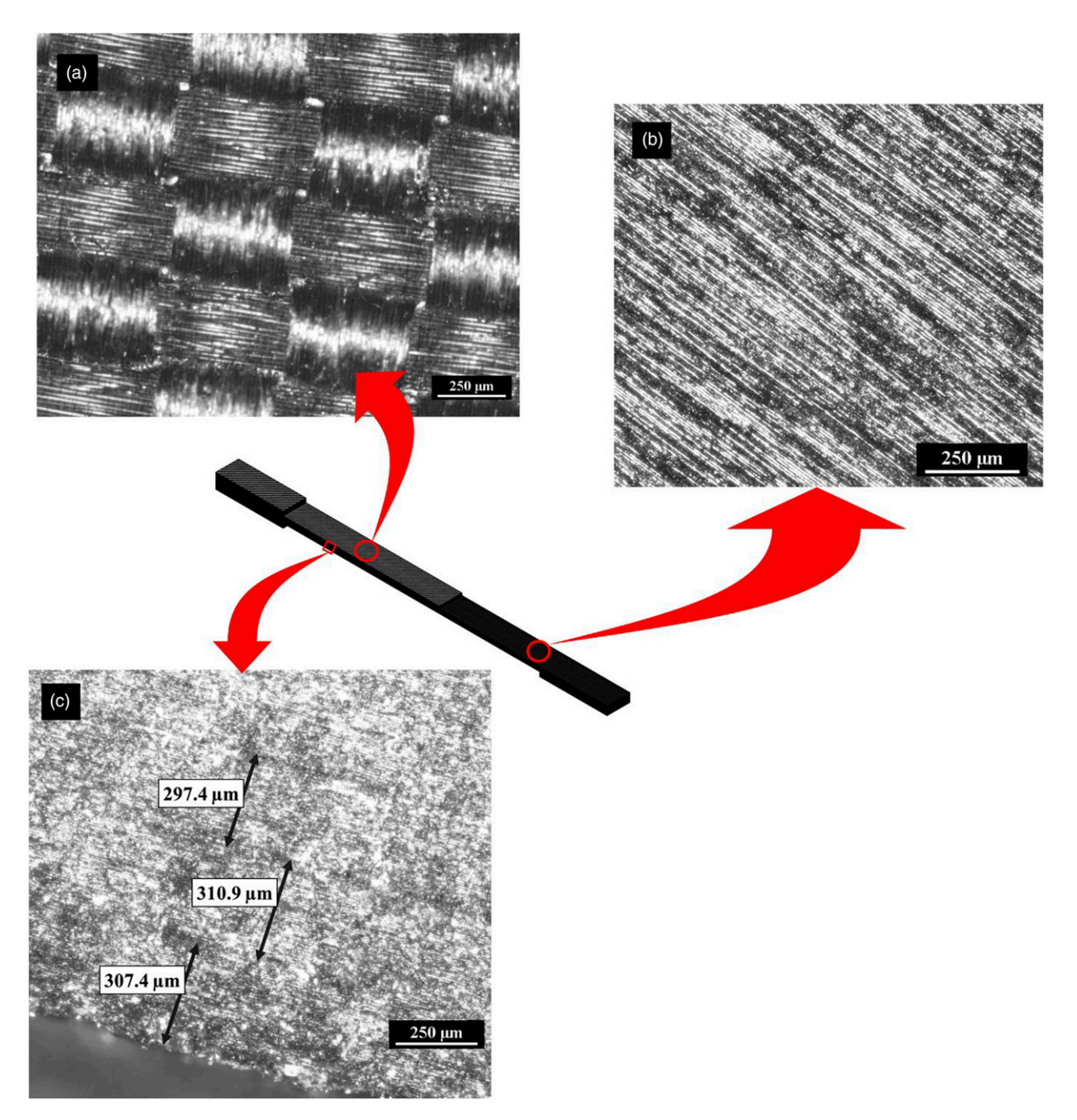


Figure 7. Five times magnified images taken from the intact sample. Here (a) is the surface layer (carbon fiber mesh), (b) is an inner layer consisting of 0° fibers, and (c) is the side view of the specimen.

in the specimen. It must be noted that for sample No. 8, the damping parameter was not applicable, as the specimen ruptured in all the layers and the layers were delaminated.

Figure 9 shows the damping variations with the impact energy to the maximum impact energy ratio (E/ E_{max}). As can be seen, the damping values can be divided into three

regions. In the first region, where corresponds to the impact energy up to $0.6~E_{\rm max}$, there is only a 3.5% increase in the damping parameter, indicating a slight change in the material's properties. A noticeable change in the damping parameter is visible for the second region that is up to $E=0.9~E_{\rm max}$. For the last region, the value of the damping

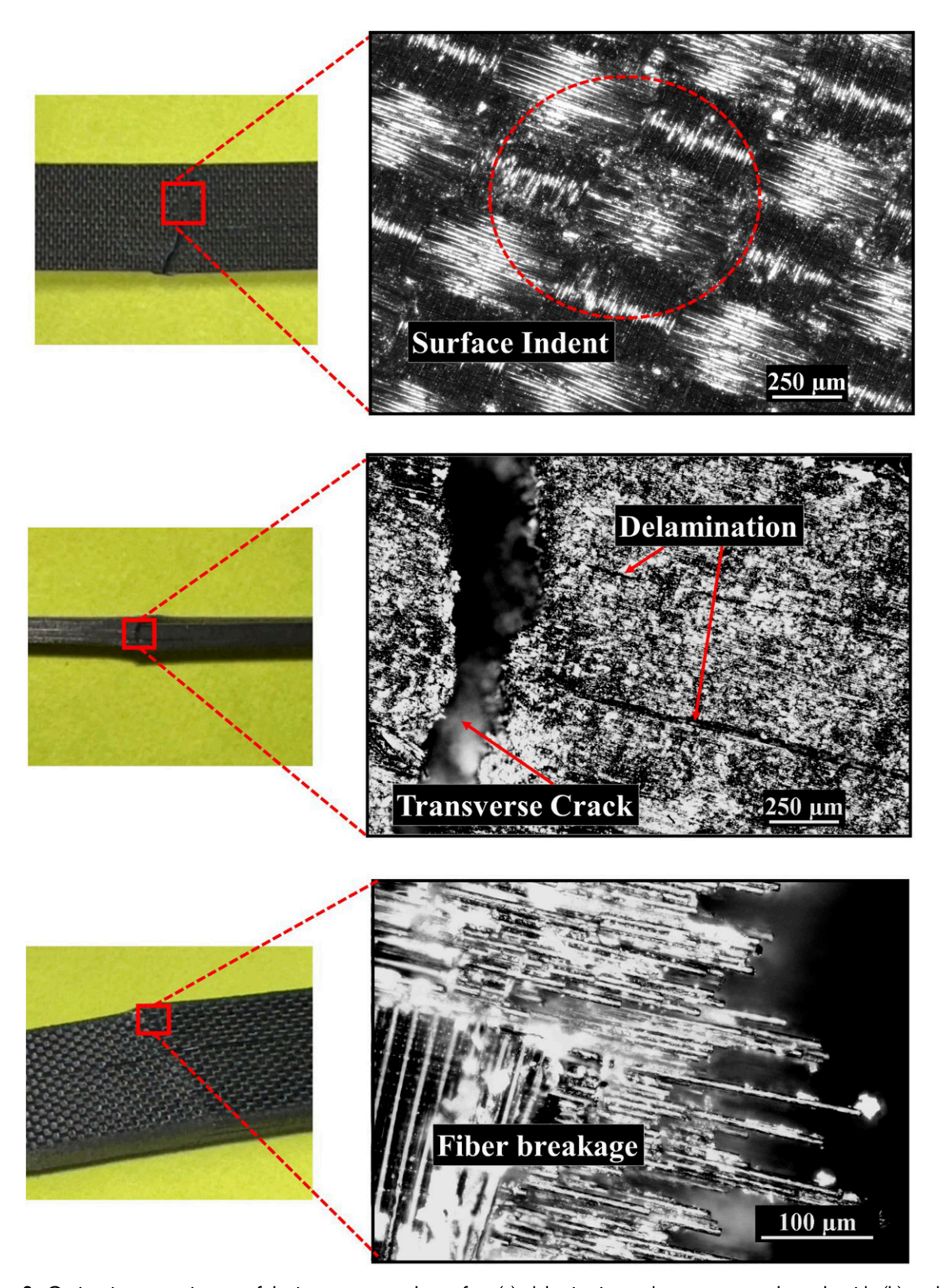


Figure 8. Optic microscope images of the impact area at the surface (a), delamination and transverse cracks at the side (b), and fiber rupture at the opposite surface (c) of the specimen with $E = E_{max}$.

Specimen no.	Impact energy (J)	Damping (Mean)×10 ⁻⁴	Damping (SD)×10 ⁻⁴	Natural frequency (mean) (Hz)	Natural frequency (SD) (Hz)
1	0	7.69	0.499	502.82	0.031
2	1.94	7.82	0.423	503.44	0.017
3	2.32	7.99	0.392	503.10	0.072
4	2.65	8.31	0.473	503.15	0.083
5	2.98	8.95	0.517	505.36	0.021
6	3.43	10.62	0.660	506.16	0.088
7	3.54	11.02	0.758	513.63	0.070

Table 3. Range and mean value of frequency and damping for specimen under different impact energy levels.

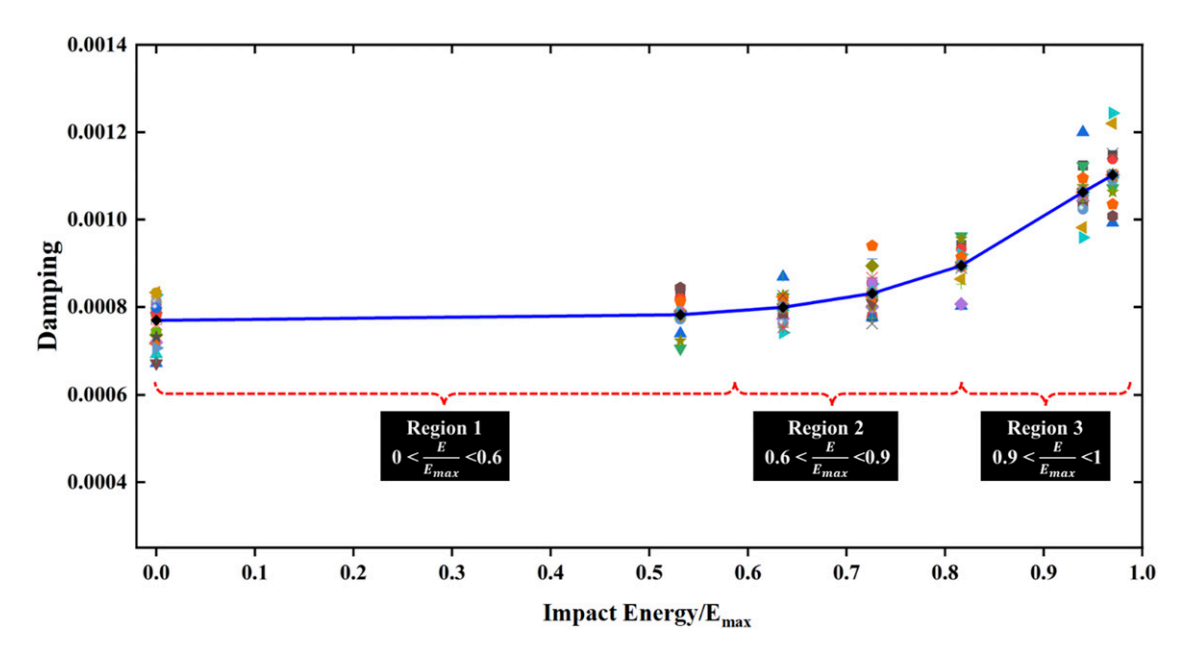


Figure 9. Variation of damping parameter with the ratio of the impact energy to the maximum energy capacity of the specimen.

Table 4. Test parameters for two tension-tension cyclic loads on CFRP specimens.

	Max stress (MPa)	Min stress (MPa)	f (Frequency) (Hz)
Test no. I	150	15	10
Test no. 2	200	20	10

parameter increases abruptly, with the slope 5.25 times the slope of region 2, revealing a significant shift in the material property. The average increase in the damping parameter between the pristine specimen and the specimen with an impact energy of 3.54 J (corresponding to E =

 $0.97~E_{max}$) is 43.3%. An increase in damping parameters by damaging the structure suggests a non-destructive method to identify damaged structures, by comparing the Q^{-I} of a given structure to the one from a pristine structure.

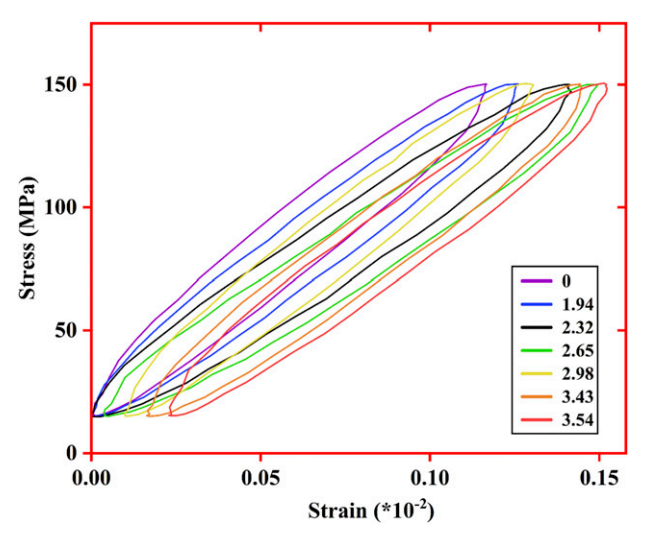


Figure 10. Cyclic stress-strain curves for specimens subjected to various low-velocity impacts under maximum stress of 150 MPa.

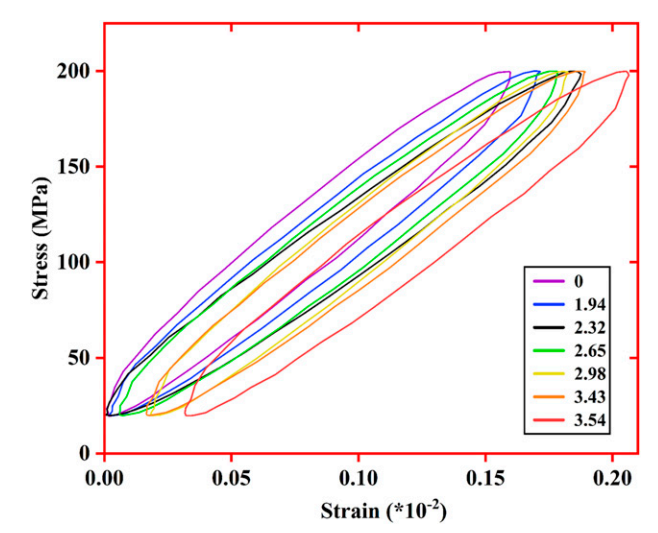


Figure 11. Cyclic stress-strain curves for specimens subjected to various low-velocity impacts under maximum stress of 200 MPa.

Hysteresis loops

In addition to calculating damping parameter variation for different impact energy levels, changes in the cyclic behavior of specimens are investigated here. The specimens were subjected to cyclic loads and stress-strain curves (Hysteresis loops) were generated. Test parameters of the two cyclic experiments on these specimens are presented in Table 4. Due to the buckling issue on CFRP specimens, cyclic tests here are limited to tension-tension testing, with the load ratio of R=0.1.

Hysteresis loops for these two experiments are presented in Figures 10 and 11, respectively, as shown below. As seen in these figures, as the impact energy increases, the stress-strain curve tends to move toward the right side. For a given stress amplitude, strains are generally higher in the specimens with a previous impact at a higher energy level.

In order to compare the damping behavior of composite specimens from the cyclic energy release standpoint, the following equation is used to calculate the damping ratio using the hysteresis loops:^{46,47}

$$\zeta = \frac{1}{4\pi} \frac{W_p}{W_e} \tag{15}$$

where *Wp* is the plastic strain energy per cycle and is equal to the area inside the hysteresis loop and *We* is elastic strain energy, the maximum elastic energy stored in each cycle and is equal to the area of a triangle surrounded by the horizontal and vertical axis and the line connecting the maximum and minimum points of the loop. For low-stress amplitudes, the area inside the loop confined by the positive axis is also known as loss energy density. In Table 5, values for plastic and elastic strain energy for each test amplitude, along with the related damping ratio, are shown.

In Figure 12, normalized values of damping ratios calculated in the table above are shown for two cases of maximum stresses equal to 150 and 200 MPa. As can be seen in this figure, although the damping ratio still demonstrates growth with the increase in the impact load, the rate of this increase is not as prominent as the findings from the IET method. Based on this figure, the hysteresis

Specimen no.	Impact energy (J)	S _{max} (MPa)	W _P (MJ/m ³)	W _e (MJ/m ³)	W _P /W _e	ζ
I	0	150	0.03135	0.083213	0.3770	0.030
		200	0.055388	0.159694	0.3468	0.0276
2	1.94	150	0.033401	0.088578	0.3775	0.030
		200	0.056072	0.154171	0.3636	0.0289
3	2.32	150	0.037662	0.094838	0.3969	0.0315
		200	0.063856	0.171844	0.3715	0.0295
4	2.65	150	0.037293	0.093944	0.3974	0.0316
		200	0.061595	0.165111	0.3732	0.0296
5	2.98	150	0.034821	0.084002	0.4147	0.0330
		200	0.056755	0.149857	0.3788	0.0301
6	3.43	150	0.036452	0.086159	0.4230	0.0336
		200	0.060227	0.156275	0.3853	0.0306
7	3.54	150	0.039292	0.08821	0.4452	0.0354
		200	0.066749	0.160377	0.4162	0.0331

Table 5. Damping ratio estimations from cyclic hysteresis loops.

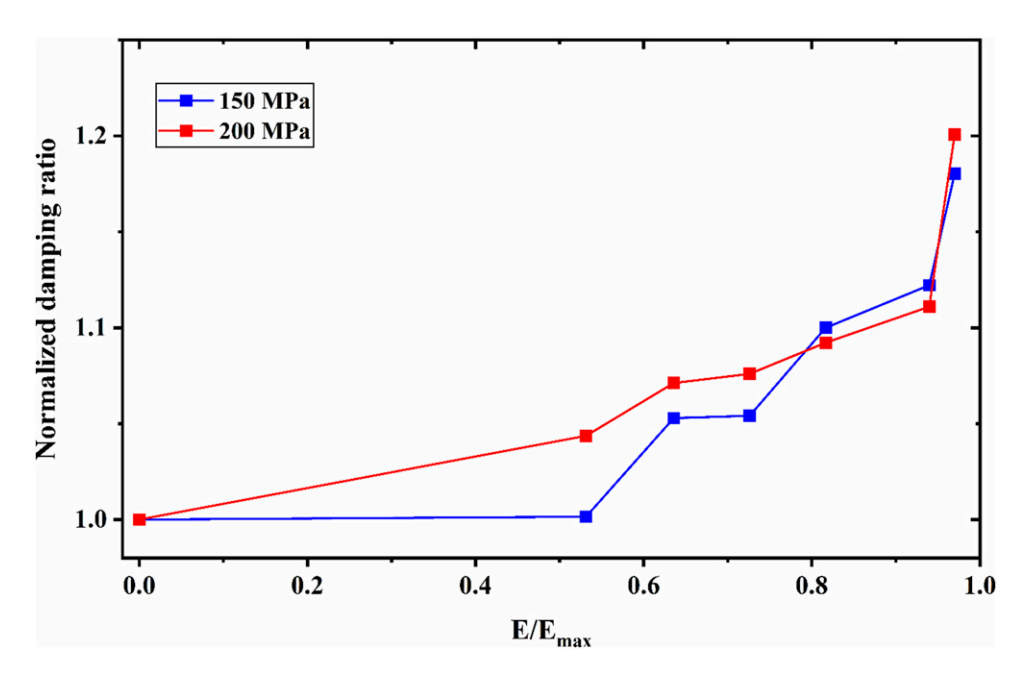


Figure 12. Variations of (normalized) damping ratio with the increase in impact energy for maximum cyclic stresses of 150 and 200 MPa.

damping ratio for the specimen with the impact energy of $0.96E_{max}$ is ~ 1.2 times the damping ratio of the pristine specimen. While the hysteresis damping approach is an indicator of increased damping with rising impact energy, the IET method is a more favorable choice primarily because it requires a simpler setup and poses a lower risk of damage during damping calculations.

Conclusions

Damage in composite materials involves complex failure modes such as delamination and transverse cracking that initiate from the inner layers of the structure, often not visible until failure occurs. This research examines the feasibility of a non-destructive method for damage detection based on the impulse excitation technique (IET). T700/T700/NCT304-1 carbon/epoxy specimens underwent low-velocity impact tests on various impact energies. The maximum impact energy for the specimen with a cross-section of 8.5×1.6 mm was 3.65 J. The coefficient of restitution decreased from 0.65 to 0.48 as the impact energy increased, indicating that a higher fraction of the impact energy is causing damaging in the specimen. All specimens were then tested in RDFA device to

acquire their damping parameter. Values of natural frequencies and damping parameters are shown in Table 3 and Figure 9. As the impact energy increases in the material, the damping parameter increases in a non-linear form. The damping value in the first region changed slightly, increasing by only 3.5% to 0.6E_{max}. With an 18% increase in the damping parameter, a more noticeable change was seen in the second region up to E = 0.9E_{max}. The damping value increases at a higher rate as impact energy reaches E_{max} and for $E > 0.9 E_{max}$ the slope was the highest. A 43.3% increase in the damping parameter was seen from E = 0 to $E = 0.97E_{max}$, indicating that the damping parameter may be used to indicate damage in CFRP parts with a relatively straightforward and non-destructive examination. These findings are supported by calculations of damping in the specimens using hysteresis loops. Specimens were subjected to two sets of tension-tension cyclic loads with S_{max} equal to 150 and 200 MPa and R = 0.1. Equation (15) was used to compute hysteresis damping, having known the stored and loss energies from the areas under and inside the hysteresis loops. As the impact energy increases, so does the specimens' damping ratio, in line with the findings from IET approaches. Interestingly, the damping for the specimen with the highest impact energy was 20% higher than for the intact specimen.

Acknowedgements

The authors wish to acknowedege partial support from NSF RII Track 1: Louisiana Materials Design Alliance (OIA-1946231) and Louisiana Board of Regents.

Declaration of conflicting interests

The author(s) declared no potential conflicts of interest with respect to the research, authorship, and/or publication of this article.

Funding

The author(s) disclosed receipt of the following financial support for the research, authorship, and/or publication of this article: This work was supported by the US National science foundation EP-SCoR; OIA-1946231. A. M. and MMK also wish to acknowedge NSF 2243755.

ORCID iDs

Ali Mahmoudi https://orcid.org/0000-0002-7109-4919 MM Khonsari https://orcid.org/0000-0003-3192-8891 G Li https://orcid.org/0000-0002-7004-6659

Data Availability Statement

Data can be made available upon request.

References

- Mahmoudi A and Mohammadi B. On the evaluation of damage-entropy model in cross-ply laminated composites. Eng Fract Mech 2019; 219: 106626.
- Prabhakar MM, Rajini M, Mayandi K, et al. An overview of burst, buckling, durability and corrosion analysis of lightweight FRP composite pipes and their applicability. *Compos Struct* 2019; 230: 111419.
- Sun G, Wang S, Hong J, et al. Experimental investigation of the quasi-static axial crushing behavior of filament-wound CFRP and aluminum/CFRP hybrid tubes. *Compos Struct* 2018; 194: 208–225.
- Ismail MF, Sultan MTBH, Hamdan A, et al. Low velocity impact behaviour and post-impact characteristics of kenaf/ glass hybrid composites with various weight ratios. *J Mater Res Technol* 2019; 8(3): 2662–2673.
- Richardson M and Wisheart M. Review of low-velocity impact properties of composite materials. *Compos Appl Sci Manuf* 1996; 27(12): 1123–1131.
- Koyanagi J, Mochizuki A, Higuchi R, et al. Finite element model for simulating entropy-based strength-degradation of carbon-fiber-reinforced plastics subjected to cyclic loadings. *Int J Fatig* 2022; 165: 107204.
- Yang B, Chen Y, Lee J, et al. In-plane compression response of woven CFRP composite after low-velocity impact: modelling and experiment. *Thin-Walled Struct* 2021; 158: 107186.
- Aoki Y, Suemasu H and Ishikawa T. Damage propagation in CFRP laminates subjected to low velocity impact and static indentation. *Adv Compos Mater* 2007; 16(1): 45–61.
- Gómez-del Rio T, Zaera R, Barbero E, et al. Damage in CFRPs due to low velocity impact at low temperature. Compos B Eng 2005; 36(1): 41–50.
- 10. Jollivet T, Peyrac C and Lefebvre F. Damage of composite materials. *Procedia Eng* 2013; 66: 746–758.
- Mahmoudi A and Khonsari MM. Evaluation of fatigue in unidirectional and cross-ply laminated composites using a coupled entropy-kinetic concept. *J Compos Mater* 2022; 56(15): 2443–2454.
- Mohammadi B and Mahmoudi A. Developing a new model to predict the fatigue life of cross-ply laminates using coupled CDM-entropy generation approach. *Theor Appl Fract Mech* 2018; 95: 18–27.
- Ghadimi H, Jirandehi AP, Nemati S, et al. Effects of printing layer orientation on the high-frequency bending-fatigue life and tensile strength of additively manufactured 17-4 PH stainless steel. *Materials* 2023; 16(2): 469.
- 14. Rouhi Moghanlou M and Saeidi Googarchin H. Threedimensional coupled thermo-mechanical analysis for fatigue failure of a heavy vehicle brake disk: simulation of braking and cooling phases. *Proc Inst Mech Eng - Part D J Automob Eng* 2020; 234(13): 3145–3163.

- Helfen T, Venkat RS, Rabe U, et al. Characterisation of CFRP through enhanced ultrasonic testing methods. *Appl Compos Mater* 2012; 19: 913–919.
- Wang B, Zhong S, Lee TL, et al. Non-destructive testing and evaluation of composite materials/structures: a state-of-the-art review. Adv Mech Eng 2020; 12(4): 1687814020913761.
- Ni Q-Q, Hong J, Xu P, et al. Damage detection of CFRP composites by electromagnetic wave nondestructive testing (EMW-NDT). Compos Sci Technol 2021; 210: 108839.
- 18. Maio L, Monaco E, Ricci F, et al. Simulation of low velocity impact on composite laminates with progressive failure analysis. *Compos Struct* 2013; 103: 75–85.
- Duffour P, Morbidini M and Cawley P. Comparison between a type of vibro-acoustic modulation and damping measurement as NDT techniques. NDT E Int 2006; 39(2): 123–131.
- Pieczonka L, Klepka A, Martowicz A, et al. Nonlinear vibroacoustic wave modulations for structural damage detection: an overview. *Opt Eng* 2016; 55(1): 011005.
- 21. Treviso A, Van Genechten B, Mundo D, et al. Damping in composite materials: properties and models. *Compos B Eng* 2015; 78: 144–152.
- 22. DeValve C and Pitchumani R. Experimental investigation of the damping enhancement in fiber-reinforced composites with carbon nanotubes. *Carbon* 2013; 63: 71–83.
- Nsengiyumva W, Zhong S, Lin J, et al. Advances, limitations and prospects of nondestructive testing and evaluation of thick composites and sandwich structures: a state-of-the-art review. *Compos Struct* 2021; 256: 112951.
- Chandra R, Singh S and Gupta K. Damping studies in fiberreinforced composites—a review. *Compos Struct* 1999; 46(1): 41–51.
- Zou S, Xiao H, Ye F, et al. Numerical analysis of the effect of the scan strategy on the residual stress in the multi-laser selective laser melting. *Results Phys* 2020; 16: 103005.
- Assarar M, El Mahi A and Berthelot J-M. Damping analysis of sandwich composite materials. *J Compos Mater* 2009; 43(13): 1461–1485.
- Khan SU, Li CY, Siddiqui NA, et al. Vibration damping characteristics of carbon fiber-reinforced composites containing multi-walled carbon nanotubes. *Compos Sci Technol* 2011; 71(12): 1486–1494.
- Kyriazoglou C, Le Page B and Guild F. Vibration damping for crack detection in composite laminates. *Compos Appl Sci Manuf* 2004; 35(7-8): 945–953.
- Yam L, Wei Z and Cheng L. Nondestructive detection of internal delamination by vibration-based method for composite plates. *J Compos Mater* 2004; 38(24): 2183–2198.
- 30. Kıral Z, İçten BM and Kıral BG. Effect of impact failure on the damping characteristics of beam-like composite structures. *Compos B Eng* 2012; 43(8): 3053–3060.

- 31. Kıral Z. Harmonic response analysis of symmetric laminated composite beams with different boundary conditions. *Sci Eng Compos Mater* 2014; 21(4): 559–569.
- 32. Berthelot J-M. Damping analysis of laminated beams and plates using the Ritz method. *Compos Struct* 2006; 74(2): 186–201.
- 33. Dieterle R and Bachmann H. Experiments and models for the damping behavior of vibrating reinforced concrete beams in the uncracked and cracked conditions. Salmon Tower Building New York City: Springer, 1981.
- Rezaee M and Hassannejad R. Free vibration analysis of simply supported beam with breathing crack using perturbation method. *Acta Mech Solida Sin* 2010; 23(5): 459–470.
- Curadelli R, Riera J, Ambrosini D, et al. Damage detection by means of structural damping identification. *Eng Struct* 2008; 30(12): 3497–3504.
- Cao M, Sha GG, Gao YF, et al. Structural damage identification using damping: a compendium of uses and features. *Smart Mater Struct* 2017; 26(4): 043001.
- Gharehbaghi VR, Farsangi EN, Noori M, et al. A critical review on structural health monitoring: definitions, methods, and perspectives. Arc Comp Met Eng, 2021; 29: 1–27.
- 38. Vahid M, Haghshenas A, Khonsari M, et al. Fatigue analysis of metals using damping parameter. *Int J Fatig* 2016; 91: 124–135.
- Zarafshan A, Ansari F and Taylor T. Field tests and verification of damping calculation methods for operating highway bridges. *Journal of Civil Structural Health Monitoring* 2014; 4: 99–105.
- Lokesh R, Jagadesh V and Suresh S. Mechanical and low velocity impact behavior of Al based kevlar fabric reinforced epoxy laminate. *Int J Appl Eng Res* 2021; 16(8): 660–669.
- 41. Sjoblom PO, Hartness JT and Cordell TM. On low-velocity impact testing of composite materials. *J Compos Mater* 1988; 22(1): 30–52.
- 42. Shivakumar K, Elber W and Illg W. Prediction of low-velocity impact damage in thin circular laminates. *AIAA J* 1985; 23(3): 442–449.
- Katsaprakakis DA, Papadakis N and Ntintakis I. A comprehensive analysis of wind turbine blade damage. *Energies* 2021; 14(18): 5974.
- Zhou G. Damage mechanisms in composite laminates impacted by a flat-ended impactor. *Compos Sci Technol* 1995; 54(3): 267–273.
- 45. Ma Q, Tan Y, Liu X, et al. Effect of coal thicknesses on energy evolution characteristics of roof rock-coal-floor rock sandwich composite structure and its damage constitutive model. *Compos B Eng* 2020; 198: 108086.
- Taborda D, Potts D and Zdravković L. On the assessment of energy dissipated through hysteresis in finite element analysis. *Comput Geotech* 2016; 71: 180–194.
- 47. Martins RF, Branco R and Long X. Fatigue life assessment in bainitic steels based on the cumulative strain energy density. *Appl Sci* 2020; 10(21): 7774.

Appendix

Appreviations

- A_i Signal amplitudes
- c Viscous damping
- e Coefficient of restitution
- E_m Young's modulus (Pa)
- E Impact energy (J)
- $E_{max} \quad \ Maximum \ impact \ capacity \ (J)$
 - h Impact height (m)

- k Spring constant
- m Mass of system (kg)
- Q Q factor
- Q^{-1} Internal friction
- UTS Ultimate tensile stress (MPa)
 - v Velocity (m/s)
 - S Logarithmic decrement
 - ζ Damping ratio
 - ρ Density (kg/m³)
 - v Poisson's ratio